

Unconventional high-temperature excitonic insulators in two-dimensional topological materials

L. Maisel Licerán^{1,*} and H. T. C. Stoof¹

¹*Institute for Theoretical Physics and Center for Extreme Matter and Emergent Phenomena, Utrecht University, Princetonplein 5, 3584 CC Utrecht, The Netherlands*

(Dated: February 3, 2025)

Bound electron-hole pairs in semiconductors known as excitons can form a coherent state at low temperatures akin to a BCS condensate. The resulting phase is known as the excitonic insulator and has superfluid properties. Here we theoretically study the excitonic insulator in a pair of recently proposed two-dimensional candidate materials with nontrivial band topology. Contrary to previous works, we include interaction channels that violate the individual electron and hole number conservations. These are on equal footing with the number-conserving processes due to the substantial overlap of Wannier orbitals of different bands, which cannot be exponentially localized due to the nontrivial Chern numbers of the latter. Their inclusion is crucial to determine the symmetry of the electron-hole pairing, and by performing mean-field calculations at nonzero temperatures we find that the order parameter is a chiral d -wave. We discuss the nontrivial topology of this unconventional state and analyze its superfluid properties. In particular, we estimate BKT temperatures between 75 K and 100 K on realistic substrates, over an order of magnitude larger than in the number-conserving approximation where s -wave pairing is favored. Our results highlight the interplay between topology at the single-particle level and long-range interactions, motivating further research in systems where both phenomena coexist.

Introduction.—Collective phenomena in many-body systems give rise to surprising material properties and new phases of matter. Prime examples are superconductivity and superfluidity, which allow for the dissipationless transport of charge and mass, respectively [1–5]. These phenomena have long been observed as a result of the condensation of Cooper pairs in metals at low temperatures. In semiconductors, fermion pairing occurs also at higher temperatures in the form of excitons, which are bound electron-hole pairs. A coherent state of excitons can form when their binding energy of these pairs exceeds the band gap energy of the semiconductor. This phase is called the excitonic insulator (EI) and could host exotic phenomena such as superfluidity [6–13].

Recent theoretical and experimental work on exciton physics has mostly focused on two-dimensional (2D) systems [14–22], which feature reduced dielectric screening of the Coulomb interaction and allow for the suppression of the radiative recombination rate via the use of spatially separated electron and hole layers. The latter is advantageous for exploring optical properties and exciton Bose-Einstein condensates, but comes at the cost of reduced exciton binding energies due to the weaker interlayer Coulomb interaction. However, the EI is a BCS-like state which appears due to an instability of the Fermi surface against spontaneous exciton formation, requiring relatively large Coulomb interactions so that the binding energies exceed the gap. The resulting phase is naturally more robust against recombination processes, and pairing with nonzero angular momentum can further increase this robustness as the correlated particles tend to avoid each other. For these reasons it is important to understand in detail the EI physics in monolayer systems, where the condition of strong Coulomb interactions can be realized more easily. As shown here, their behavior can differ greatly from that in bilayer systems, with non- s -wave condensation realized in the presence of topology.

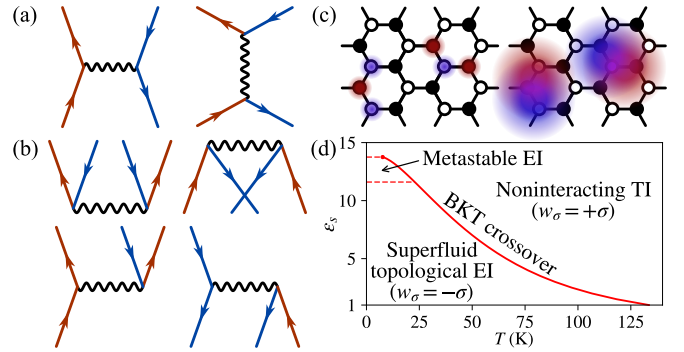


FIG. 1. (a) Examples of U(1)-symmetric scattering channels, where the number of ingoing electrons (red lines) is equal to that of outgoing ones, and similarly for the holes (blue lines). (b) Examples of U(1)-breaking scattering processes which do not conserve the individual electron and hole numbers. (c) Sketch of Wannier orbitals in the case of trivial bands (left) and bands with a nonzero Chern number (right). Due to the nonlocalizability of the latter, orbitals corresponding to the conduction and valence bands have significant mutual overlaps in coordinate space and the processes depicted in (b) become relevant. (d) Phase diagram of MTCO in the ϵ_s - T plane, where ϵ_s is the dielectric constant of the material substrate. At low ϵ_s and T we find a topological $d + id$ singlet EI whose winding number w_σ in each spin subspace σ is opposite to that of the underlying noninteracting TI at high ϵ_s or T . This EI has a superfluid response, even though it shares the same symmetries as the underlying TI due to the explicit U(1) breaking caused by the diagrams in (b). As a result, the BKT transition calculated here via the standard theory becomes only a smooth crossover and is accompanied by a gap closing in its vicinity which connects the two topologically distinct phases.

We consider the EI in topological monolayer materials with a band inversion accompanied by a phase winding of the electron and hole states around a high-symmetry point [23–25]. Because the bands in such systems possess a nonzero Chern number, the associated Wannier orbitals are weakly localized [26, 27]. When considering Coulomb interactions, this fea-

* l.maiselliceran@uu.nl

ture manifests in the appearance of scattering processes where the involved quasiparticles can switch bands at the electrostatic vertex, thus breaking the individual electron and hole U(1) symmetries. In Fig. 1b we show some examples of these U(1)-breaking channels. Furthermore, the phase winding of the single-particle wave functions causes these channels to couple together different angular momenta, in turn influencing the pairing symmetry of the electron-hole order parameter.

In this work we consider the topological 2D materials AsO and Mo₂TiC₂O₂ (MTCO) introduced in Ref. [28], which feature such a band inversion around the Γ point and whose conduction and valence bands closest to the Fermi surface have unit Chern numbers [29]. In these systems, these two bands have equal parity at the Γ point, which inhibits dipole transitions between them. As a result, the screening of the Coulomb interaction is largely independent of the magnitude of the band gap, which allows for exciton binding energies larger than the gap [30]. Ref. [28] only included the U(1)-symmetric channels of Fig. 1a on top of the noninteracting bands, where the character of a particle (electron or hole) is conserved at the electrostatic vertex, an approach which is in fact ubiquitous [8, 13, 28, 31–33]. Here we show that including all additional U(1)-breaking channels leads to a topological $d + id$ spin-singlet EI, whereas the number-conserving approximation gives an s -wave order parameter in the triplet channel.

An important tuning parameter in our calculations is the dielectric constant ϵ_s of the substrate below the material sample. Above a certain material-dependent critical value, the dielectric screening of the electron-hole interaction is too strong to sustain an EI and we obtain the band structure of the underlying noninteracting semiconductor, which we refer to as the topological insulator (TI) phase. The TI and the EI share the same symmetries due to the inevitable presence of the U(1)-breaking terms. As a result, the superfluid density carried by the excitonic (quasi)condensate can never fully vanish, hence the TI must always have an extremely small, but technically nonzero superfluid response. Accordingly, the Berezinskii-Kosterlitz-Thouless (BKT) mechanism now leads to a smooth crossover instead of a true phase transition. In Fig. 1d we show the phase diagram of MTCO in the ϵ_s - T plane. We have estimated that the EI in both materials remains robust up to temperatures as high as 75 K on realistic substrates, making these systems potential candidates for high-temperature superfluid heat transport.

Low-energy model.—The materials under consideration are described by a low-energy Hamiltonian $H_0(\mathbf{k}) = \text{diag}[h_+(\mathbf{k}), h_-(\mathbf{k})]$ that correctly reproduces the GW band structure around the Γ point [28]. Here,

$$h_\sigma(\mathbf{k}) = \begin{bmatrix} h_0(k) + \sigma\lambda & \alpha k_-^2 \\ \alpha k_+^2 & h_0(k) - \sigma\lambda \end{bmatrix}, \quad (1)$$

with $k_\pm = k_x \pm ik_y$, $k = |\mathbf{k}|$, and $h_0(k) = \epsilon_0 + ck^2$. The diagonal blocks of $H_0(\mathbf{k})$ describe spin-up and spin-down electrons ($\sigma = \pm$, respectively) in a basis of $p_x \pm ip_y$ ($d_{xy} \pm id_{x^2-y^2}$) orbitals for AsO (MTCO). The bands of h_σ have a gap of magnitude 2λ at $k = 0$ and feature nontrivial Chern numbers $C = \pm\sigma \text{sgn } \lambda$, with opposite signs for each type of band in the two spin subspaces due to the time-reversal symmetry.

On top of this single-particle picture we consider the repulsive Coulomb interaction $\hat{V} = \frac{1}{2\mathcal{A}} \sum_{\mathbf{q}} \hat{n}_{\mathbf{q}} V(\mathbf{q}) \hat{n}_{-\mathbf{q}}$, with $\hat{n}_{\mathbf{q}}$ the Fourier-transformed density operator in the orbital-spin basis corresponding to the Γ -point eigenstates and \mathcal{A} the surface area of the system. It can be shown on very general grounds that this form of the interaction must be written in our basis states at the Γ point, which in turn leads to the U(1)-breaking terms. Due to the 2D geometry we neglect screening of the Coulomb interaction, but we do include polarization and substrate effects by taking $V(\mathbf{q}) = 2\pi/[q(\epsilon + 2\pi\alpha_{2D}q)]$. Here α_{2D} is the 2D polarizability of the medium, and $\epsilon = (1 + \epsilon_s)/2$ is the average between the dielectric constant ϵ_s of the substrate below the sample and the vacuum above. We also exclude electron-phonon coupling because it effectively leads to U(1)-breaking terms like the ones we already consider [34], and hence such a coupling will at most lead to a channel-dependent ϵ that leaves the qualitative picture unchanged. The numerical values of the model parameters in atomic units [35] are $\lambda = 0.0030$, $c = 0.198$, $\alpha = -0.534$, $\alpha_{2D} = 38.7$ for AsO, and $\lambda = 0.0021$, $c = -1.251$, $\alpha = 1.602$, $\alpha_{2D} = 19.7$ for MTCO.

U(1)-breaking terms in the TI phase.—Before addressing their consequences on the EI, we briefly explore the effect of the U(1)-breaking channels on excitons in the TI state. In this context, neglecting them is known as the Tamm-Dancoff approximation (TDA) for the excitonic Bethe-Salpeter equation (BSE). The TDA drops the U(1)-breaking coupling between resonant and antiresonant processes in the calculation of exciton spectra and keeps only U(1)-symmetric processes [36–41]. This is appropriate when the resonant and antiresonant subspaces are far away in energy, which in particular holds when the exciton binding energies ϵ_b are much smaller than the semiconductor band gap E_g . In this case, $\kappa^2\epsilon_b/2E_g \ll 1$, with κ a characteristic overlap between the valence and conduction wave functions. However, if the binding energy of excitons becomes comparable to the gap, the resonant-antiresonant coupling becomes important. For this reason we expect the U(1)-breaking channels to influence the onset of the EI phase, and the question arises whether they also play a role on the properties of the EI at low temperatures.

The full BSE goes beyond the variational exciton state $|X_\Phi\rangle = \sum_{c\nu k} \Phi_k^{c\nu} \hat{\psi}_{c\nu}^\dagger \hat{\psi}_{\nu k} |DS\rangle$, which automatically leads to the TDA for the envelope wave function Φ . Here, c (ν) represents an arbitrary conduction (valence) band with corresponding creation and annihilation operators $\hat{\psi}_{c(\nu)\mathbf{k}}^\dagger$ and $\hat{\psi}_{c(\nu)\mathbf{k}}$, respectively, and $|DS\rangle$ is the semiconductor's Dirac-sea ground state. The full BSE for the exciton spectra at $T = 0$ is given by the generalized eigenvalue problem [36–41]

$$\begin{bmatrix} H^{(\text{res})} & \bar{V} \\ \bar{V}^* & [H^{(\text{res})}]^* \end{bmatrix} \begin{bmatrix} \Phi \\ \bar{\Phi} \end{bmatrix} = \omega \begin{bmatrix} \mathbb{I} & 0 \\ 0 & -\mathbb{I} \end{bmatrix} \begin{bmatrix} \Phi \\ \bar{\Phi} \end{bmatrix}, \quad (2)$$

with an implied summation over internal bands and momenta. The resonant part is $H_{c\nu c' \nu'}^{(\text{res})}(\mathbf{k}, \mathbf{k}') = \delta_{\mathbf{k}\mathbf{k}'} \delta_{c\nu c'} \delta_{\nu\nu'} (\epsilon_{\mathbf{k}}^c - \epsilon_{\mathbf{k}'}^{\nu'}) - \frac{1}{\mathcal{A}} V_{c\nu c' \nu'}^D(\mathbf{k}, \mathbf{k}')$, while $\bar{V}_{c\nu c' \nu'}(\mathbf{k}, \mathbf{k}') = -\frac{1}{\mathcal{A}} V_{c\nu \nu' c'}^D(\mathbf{k}, \mathbf{k}')$ is the resonant-antiresonant coupling. Here, $\epsilon_{\mathbf{k}}^\alpha$ and $|u_{\mathbf{k}}^\alpha\rangle$ are the single-particle energies and eigenstates, and the so-called direct interaction reads [42, 43]

$$V_{\alpha\beta\alpha'\beta'}^D(\mathbf{k}, \mathbf{k}') = V(\mathbf{k} - \mathbf{k}') \langle u_{\mathbf{k}}^\alpha | u_{\mathbf{k}'}^{\alpha'} \rangle \langle u_{\mathbf{k}'}^{\beta'} | u_{\mathbf{k}}^\beta \rangle. \quad (3)$$

For the model of Eq. (1), α, β, \dots take values in $\{c, v\} \times \{\uparrow, \downarrow\}$. We see that \bar{V} represents the ‘‘vacuum-to-pair’’ processes in the first row of Fig. 1b, which break the individual U(1) symmetries. In general one should also include the exchange interaction, but this vanishes here as we only consider excitons with zero total momentum [42–44].

The exciton states are classified in the orthogonal spin configurations $|c\uparrow, v\uparrow\rangle$ and $|c\uparrow, v\downarrow\rangle$, corresponding to antiparallel and parallel spins for the electron and the hole, respectively. We have calculated the exciton energies of each subspace for values of ε_s up to 7 and found that the ground-state energies are all larger than the gap, indicating a potential excitonic instability. We define $\Delta E = E_{\uparrow\uparrow} - E_{\uparrow\downarrow}$ as the energy difference between the antiparallel and parallel configurations. In the TDA, the antiparallel sector lies slightly higher in energy, with $\Delta E_{\text{AsO}}^{\text{TDA}} \approx 0.9(3)$ meV and $\Delta E_{\text{MTCO}}^{\text{TDA}} \approx 4.1(2)$ meV. Remarkably, this ordering inverts under the inclusion of the resonant-antiresonant coupling, giving $\Delta E_{\text{AsO}}^{\text{BSE}} \approx -0.32(8)$ meV and $\Delta E_{\text{MTCO}}^{\text{BSE}} \approx -0.35(9)$ meV [45]. This gives a first indication that condensation with antiparallel spins may be favored over the pure triplet channel found in Ref. [28] in the presence of U(1)-symmetric channels only, which we now verify by explicitly solving the mean-field equations.

Mean-field theory.—We now study the EI phase in these materials via mean-field theory at $T \geq 0$. After a Hartree-Fock treatment of the interaction we identify the gap parameters

$$\Delta_{\mathbf{k}}^{\alpha\beta} = -\frac{1}{\mathcal{A}} \sum_{\alpha'\beta'k'} V_{\alpha\beta\alpha'\beta'}^{\text{D}}(\mathbf{k}, \mathbf{k}') \rho_{k'}^{\alpha'\beta'}, \quad (4)$$

with $\rho_{\mathbf{k}}^{\alpha\beta} = \langle \hat{\psi}_{\beta\mathbf{k}}^\dagger \hat{\psi}_{\alpha\mathbf{k}} \rangle - \delta_{\alpha\beta} \delta_{\alpha,v}$ the density matrix relative to the Dirac sea. We find mean-field configurations by iterating over pairs (Δ, ρ) until the free energy has converged, using that $\langle \hat{\psi}_{\beta\mathbf{k}}^\dagger \hat{\psi}_{\alpha\mathbf{k}} \rangle = \sum_{\gamma} [\mathcal{U}_{\mathbf{k}}^{\Delta}]_{\alpha\gamma} N_{\text{F}}(\omega_{\mathbf{k}}^{\gamma} - \mu) [\mathcal{U}_{\mathbf{k}}^{\Delta}]_{\gamma\beta}^{\dagger}$. Here, $N_{\text{F}}(x) = (e^{\beta x} + 1)^{-1}$ is the Fermi-Dirac distribution, $\mathcal{U}_{\mathbf{k}}^{\Delta}$ the matrix diagonalizing the mean-field Hamiltonian $\mathcal{H}_{\alpha\beta}^{\Delta}(\mathbf{k}) = \delta_{\alpha\beta} \varepsilon_{\mathbf{k}}^{\alpha} + \Delta_{\mathbf{k}}^{\alpha\beta}$ with eigenvalues $\omega_{\mathbf{k}}^{\alpha}$, and μ the chemical potential which is found by imposing charge neutrality.

For large ε_s we recover the underlying TI at all temperatures, while for small enough ε_s we find an EI. The transition as a function of ε_s is of first order, compatible with the fact that the two phases share the same symmetries due to the presence of the U(1)-breaking terms. The EI obtained here is more robust than in the number-conserving approximation, with critical dielectric constants $\varepsilon_{s,c}^{\text{AsO}} \approx 7.1$ and $\varepsilon_{s,c}^{\text{MTCO}} \approx 11.6$ at $T = 0$, which are higher than those reported in Ref. [28]. Furthermore, they exist in a metastable state up to $\varepsilon_{s,m}^{\text{AsO}} \approx 9.2$ and $\varepsilon_{s,m}^{\text{MTCO}} \approx 13.7$. In Fig. 2 we present the excitonic gap parameter and quasiparticle dispersions at $T = 0$. We obtain $\Delta_{\mathbf{k}}^{\alpha\beta} = 0$ for all channels where the spins of bands α and β are antiparallel. By contrast, $\Delta_{\mathbf{k}}^{c\uparrow v\uparrow} = \Delta(k) k_{\perp}^2$ with $\Delta(k)$ a decreasing function of k . Meanwhile, the diagonal components are of s -wave type and satisfy $\Delta_{\mathbf{k}}^{c\uparrow c\uparrow} = -\Delta_{\mathbf{k}}^{v\uparrow v\uparrow}$. The gap parameters in the spin-down subspace are the complex conjugates of the spin-up ones and the density matrix has the same form.

These results can be contrasted with Ref. [28], where the gap parameter is an s -wave triplet in the channels $(c\uparrow, v\downarrow)$ and

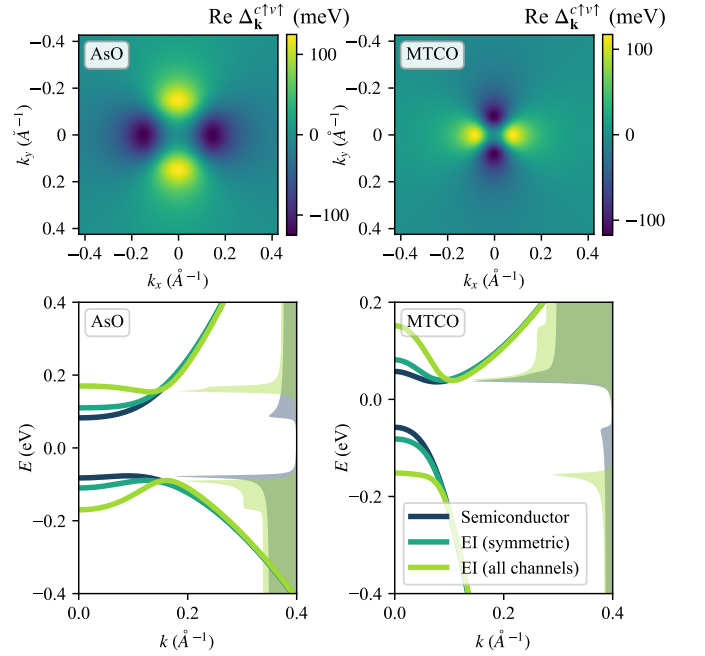


FIG. 2. Real part of the gap function $\Delta_{\mathbf{k}}^{c\uparrow v\uparrow} \propto k_{\perp}^2$ (top) and quasiparticle dispersions (bottom) for both materials. We compare the dispersions in the presence of all channels and of U(1)-symmetric processes only. In the former case the gap is topological and is widened by the diagonal gap parameters $\Delta_{\mathbf{k}}^{c\uparrow c\uparrow}$ and $\Delta_{\mathbf{k}}^{v\uparrow v\uparrow}$. The right side of the plots show the density-of-states profiles of the TI and of our $d + id$ EI. Here we have used $\varepsilon_s = 4$ for AsO and $\varepsilon_s = 7$ for MTCO.

$(c\downarrow, v\uparrow)$, with $\Delta_{\mathbf{k}}^{c\uparrow v\uparrow} = \Delta_{\mathbf{k}}^{c\downarrow v\downarrow} = 0$. The discrepancy arises due to the U(1)-symmetric approximation for the interaction matrix where only $V_{cv'c'v'}^{\text{D}}$ is kept, which is not permissible here owing to the phase winding of $H_0(\mathbf{k})$. The latter imbues the bare interaction with a d -wave structure that is inequivalent for the different channels. The U(1)-symmetric scattering alone is compatible with any angular momentum via Eq. (4), and the corresponding s -wave solution has the lowest energy. However, the U(1)-breaking terms spoil this compatibility and thus preclude a pure s -wave order parameter. Crucially, processes such as those of the second row of Fig. 1b couple the diagonal and off-diagonal elements of the density matrix. In other words, a nonzero $\rho_{\mathbf{k}}^{c\uparrow c\uparrow}$ always leads to a nonzero $\Delta_{\mathbf{k}}^{c\uparrow v\uparrow}$. Similar considerations hold for the spin-down subspace. The result is that $\Delta_{\mathbf{k}}^{c\uparrow v\uparrow} = \Delta_{\mathbf{k}}^{c\downarrow v\downarrow} = 0$ is not possible in the EI in the presence of all channels while $\Delta_{\mathbf{k}}^{c\uparrow v\downarrow} = \Delta_{\mathbf{k}}^{c\downarrow v\uparrow} = 0$ is permissible, meaning that the spin-U(1) and time-reversal symmetries are both preserved. Hence, including all available interaction channels into the self-consistent mean-field calculation can dramatically influence the ground state. Our results are robust as long as $V(\mathbf{q})$ depends solely on $|\mathbf{q}|$ and the potential in coordinate space has a long-range tail. It is important to realize that a contact potential can lead to artificial results in the presence of nontrivial winding of the single-particle states, as the latter will in general couple to the nonzero angular-momentum components of $V(\mathbf{q})$. Despite the fact that we work in the

long-wavelength limit, the last statement also translates to lattice models: in the presence of topology it is in general not enough to consider the on-site repulsion only, and one should at least take nearest-neighbor interactions into account.

The chiral d -wave symmetry of the gap arises due to the hybridizing terms k_{\pm}^2 in the single-particle Hamiltonian, which propagate into the interaction matrix. From our analysis it follows that a winding w will lead to interband gap parameters proportional to $(k_x \pm ik_y)^w$ with antiparallel electron-hole spins. A p -wave EI arises for $w = 1$, which corresponds to a massive Dirac model. Note that a p -wave singlet EI is allowed because electrons and holes are nonidentical particles with less restrictive pairing symmetries than ordinary superconductors. In this sense, the EI is akin to a multiband BCS state.

Topological properties.—To study the topology of this EI we firstly focus on the Chern numbers of the quasiparticle bands, which remain well-defined due to the block-diagonal form of the mean-field Hamiltonian in the EI phase. The quasiparticle dispersions read $\omega_{\mathbf{k}}^{\pm} = \frac{1}{2}[\varepsilon_{\mathbf{k}}^c + \varepsilon_{\mathbf{k}}^v \pm \sqrt{(\varepsilon_{\mathbf{k}}^c - \varepsilon_{\mathbf{k}}^v)^2 + 4|\Delta_{\mathbf{k}}^{cv}|^2}]$, where $\varepsilon_{\mathbf{k}}^{\alpha} = \varepsilon_{\mathbf{k}}^{\alpha} + \Delta_{\mathbf{k}}^{\alpha\alpha}$. Here we implicitly take equal spins for c and v and omit the label. In the presence of nontrivial gap parameters, the Chern numbers are

$$C = \pm\sigma \operatorname{sgn}(\varepsilon_0^c - \varepsilon_0^v) \operatorname{sgn} \lambda. \quad (5)$$

The parameter λ was introduced in Eq. (1) and in our case is positive for both systems. The Chern numbers become opposite to the TI ones whenever the quasiparticle gap is inverted, i.e., $\Delta_0^{cc} = -\Delta_0^{vv} < -(\varepsilon_0^c - \mu) < 0$. As shown in Fig. 1d, this is the case in a large region of the parameter space (ε_s, T) , and thus we can distinguish the EI and the TI via different topological invariants even though they share the same symmetries.

To further understand the topological properties we connect the density matrix with the BCS-like ground state $|\Psi_{\text{EI}}\rangle = \prod_{\mathbf{k}\sigma} (u_{\mathbf{k}}^{\sigma} + v_{\mathbf{k}}^{\sigma} \hat{\psi}_{c\mathbf{k}\sigma}^{\dagger} \hat{\psi}_{v\mathbf{k}\sigma}) |DS\rangle$ via $\rho_{\mathbf{k}}^{c\sigma, c\sigma} = -\rho_{\mathbf{k}}^{v\sigma, v\sigma} = |v_{\mathbf{k}}^{\sigma}|^2$ and $\rho_{\mathbf{k}}^{c\sigma, v\sigma} = v_{\mathbf{k}}^{\sigma} (u_{\mathbf{k}}^{\sigma})^*$. Defining $g_{\mathbf{k}}^{\sigma} = v_{\mathbf{k}}^{\sigma} / u_{\mathbf{k}}^{\sigma}$ we find $g_{\mathbf{k}}^{\sigma} \propto (k_x + i\sigma k_y)^{-2}$ around the origin. This corresponds to the weak-pairing abelian phase described in Refs. [46, 47], and following similar arguments we conclude that there must exist fermionic bound states at the edges of a sample, which will be helical due to the preserved time-reversal symmetry. However, the same is true for the TI, so experimentally it would be difficult to distinguish between these two phases on the basis of the density of states at the edge of a sample on a homogeneous substrate. Nevertheless, we can exploit the opposite winding numbers of the high- and low- ε_s phases to propose an experimental setup capable of distinguishing between the TI phase and the $d + id$ EI as follows.

We assume that the candidate material is placed on top of a substrate with a position-dependent dielectric constant, which we take as $\varepsilon(y < 0) = \varepsilon_L > \varepsilon_{s,c}$ and $\varepsilon(y > 0) = \varepsilon_R < \varepsilon_{s,c}$. For $y \gg 0$ the system is in the EI phase, while for $y \ll 0$ it lies in the TI regime. The winding numbers of these phases differ by two, and thus by the bulk-boundary correspondence we expect two pairs of helical edge states located at the interface between the two regions. These can be found by matching the solutions of H_0 for $y < 0$ with those of $\mathcal{H}^{\Delta} = H_0 + H_F$ for $y > 0$, where H_F is the Fock Hamiltonian containing the nontrivial

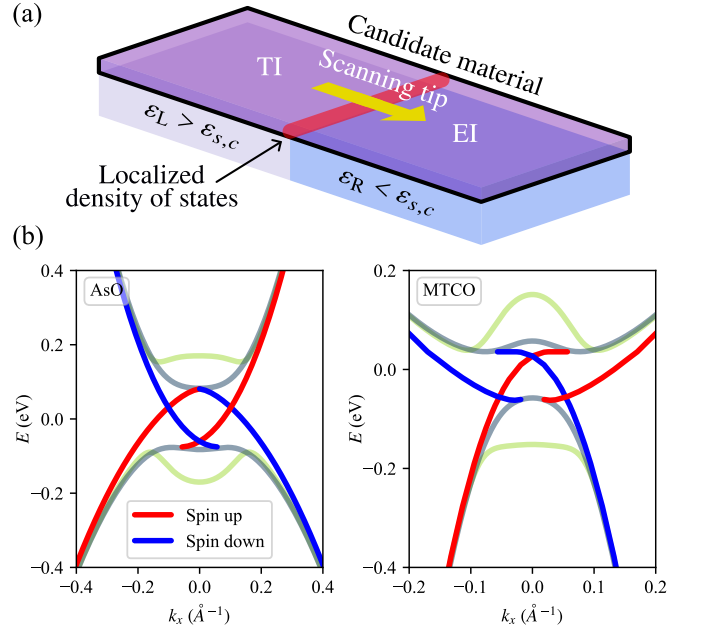


FIG. 3. (a) Experimental setup described in the main text. The left side of the candidate material lies on a substrate of high dielectric constant, while the substrate on the right side has low ε_s . We then have different topological phases at both sides, in particular $x \gg 0$ contains the EI phase. This leads to localized topological states at the interface between both regions which can be detected experimentally by scanning the density of states across the interface at energies lying inside the band gap. (b) Approximate band structure of the proposed system showing two pairs of helical edge modes crossing the band gap. While not shown here, their wave functions are localized at the interface and decay exponentially away from it.

gap parameters. While solving the full model is difficult due to the complicated \mathbf{k} -dependence of the many-body gap, to obtain a qualitative picture we can approximate the Hamiltonian for $y > 0$ as H_0 with the substitution $\lambda \rightarrow \lambda + \Delta_0^{cc}$. This preserves the crucial effect of the nontrivial gap parameters in H_F , which is to invert the gap in the topological EI regime, while preserving the low- and high- \mathbf{k} dependence of the quasiparticle dispersions and wave functions. Meanwhile, the behavior at intermediate momenta is irrelevant for our purposes because it may be obtained via a continuous deformation. We then change $k_y \rightarrow -i\partial_y$ and perform a Jackiw-Rebbi-like calculation [48] yielding the bands shown in Fig. 3b, which conform to our expectations. We note that the same can be achieved by placing the sample on a homogeneous substrate with an additional dielectric on top of half the sample in such a way that the total effective dielectric constants at both sides still satisfy our requirements, which may be more feasible experimentally.

Superfluidity.—We have also computed the bare superfluid weight D_s [49–52] for our d -wave EI as well as for the s -wave ground state in the U(1)-conserving approximation. The results are plotted in Fig. 4 and show that D_s for our topological d -wave EI is dramatically enhanced with respect to the U(1)-symmetric case. This leads to high-temperature BKT transitions in both materials on realistic substrates with relatively large dielectric constant, at least under the Nelson-Kosterlitz

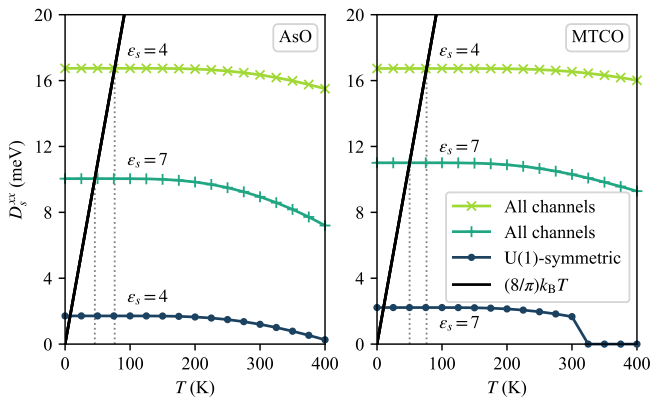


FIG. 4. Superfluid weight as a function of temperature and visualization of T_{BKT} via the Nelson-Kosterlitz criterion for substrate dielectric constants $\epsilon_s = 4, 7$. The latter is slightly higher than that of the hexagonal boron nitride and gives T_{BKT} between 45 and 50 K, making these EIs high-temperature exciton superfluids on a realistic substrate. We also show D_s for the EI with only U(1)-symmetric channels included, whose T_{BKT} is of at most a few Kelvin.

criterion for estimating T_{BKT} which employs the unrenormalized superfluid weight [53, 54]. For this calculation we ignore the self-consistency of the gap parameters derived from the microscopic model and instead treat them as fixed, as is often done for simplicity. Also, we only consider the conventional part of the superfluid weight, which is safe since the dispersions are not flat [55]. We further note that the traditional BKT theory can in principle be employed in U(1)-invariant systems only. Our calculation thus assumes that the strength of the U(1)-breaking terms is small compared to the number-conserving channels, which we expect to be the case since they all involve overlaps between different bands. From this perspective, the effect of adding the U(1)-breaking channels is to make the $d+id$ EI the only possible solution, and its superfluid weight is what we compute here. While there is a large superfluid density, the presence or absence of perfect superfluid flow will ultimately depend on the relative strength between the U(1)-conserving and U(1)-breaking processes [56]. Finally, we note that the superfluid response must be probed in terms of a heat current and not an electric current, as the usual drag and counterflow experiments are not possible monolayers.

Discussion and outlook.—In summary, we have studied the EI phase in two recently proposed candidate materials in the presence of symmetry-breaking interaction channels which arise due to the inherent nonlocalizability of the Wannier functions associated to topological bands. While in the TI phase these channels merely refine the calculation of exciton spectra, in an EI phase they can be paramount to obtain the correct ground-state configuration. Due to the U(1)-breaking terms we obtain an unconventional exciton pairing whose angular momentum is determined by the phase winding of the free electrons and in the cases considered here corresponds to $d+id$ order parameters. The corresponding EI is topologically non-trivial and distinct from the TI phase, a property that we have employed to propose an experimental setup capable of distin-

guishing between the two via density-of-states measurements in the considered systems. The EI found here also displays a large superfluid weight leading to a high-temperature BKT crossover in the vicinity of 75 K in both materials on experimentally achievable substrates.

The results reported in this work all refer to condensation with vanishing total exciton momentum, $\mathbf{K} = \mathbf{0}$. However, we expect the U(1)-breaking terms to also play a role in the condensation at nonzero \mathbf{K} , where previous research has shown that even in the semiconductor state it can be important to go beyond them [39]. A first result in this regard is that the Larkin-Ovchinnikov phase $\Delta_{\mathbf{K}_0}^{cv}(\mathbf{R}) \propto \cos(\mathbf{K}_0 \cdot \mathbf{R})$ (with \mathbf{R} the coordinate-space center of mass) should appear instead of the Fulde-Ferrel phase $\Delta_{\mathbf{K}_0}^{cv}(\mathbf{R}) \propto e^{i\mathbf{K}_0 \cdot \mathbf{R}}$, as the U(1)-breaking channels couple the $\pm\mathbf{K}$ components of the density matrix. Nonzero- \mathbf{K} exciton condensation should naturally occur in systems where the single-particle band structure has a pronounced camelback shape, and has also been recently engineered experimentally [57]. However, in the latter experiment the electrons and holes are confined to spatially separated layers and thus the effect of the U(1)-breaking terms is negligible.

While our work focuses on the EI state, the dressing of the effective electron-electron interaction with hybridization effects leading to U(1)-breaking channels is a universal mechanism. Our theory applies to pairing of quasiparticles in topological bands with nonzero Chern number whose Wannier orbitals have significant overlaps, but more generally it can have implications whenever there is significant band curvature around the center of the relative wave function of the bound quasiparticles, as the former will generally affect the properties of the Wannier orbitals. In particular it can be relevant for multi-band superconductors, in which case breaking of the total charge conservation can still occur, but with the pairing being influenced by the presence of the U(1)-breaking terms associated to the individual bands. In this regard we emphasize that our model calculation of the EI properties naturally leads to a chiral d -wave gap even though the U(1)-symmetric part of the density-density interaction alone would generally favor s -wave pairing. Our findings suggest that unconventional pairing should be rather ubiquitous when topological bands are involved and may go hand in hand with a large superfluid response. We hope this will further motivate the search of exotic phases of matter in systems hosting both topological properties and long-range interactions.

Acknowledgments—We are indebted to the authors of Ref. [28] for providing the numerical values of the $\mathbf{k} \cdot \mathbf{p}$ model parameters for AsO and MTCO. We also thank Daniel Vanmaekelbergh and Ingmar Swart for useful discussions, as well as Lumen Eek for a suggestion regarding the experimental proposal. This work is supported by the Delta-ITP consortium and by the research program *QuMat – Materials for the Quantum Age*. These are programs of the Netherlands Organisation for Scientific Research (NWO) and the Gravitation program, respectively, which are funded by the Dutch Ministry of Education, Culture, and Science (OCW).

- [1] J. Bardeen, L. N. Cooper, and J. R. Schrieffer, *Physical Review* **108**, 1175 (1957).
- [2] M. Tinkham, *Introduction to superconductivity*, Vol. 1 (Courier Corporation, 2004).
- [3] J. F. Annett, *Superconductivity, superfluids and condensates*, Vol. 5 (Oxford University Press, 2004).
- [4] A. J. Leggett, *Quantum liquids: Bose condensation and Cooper pairing in condensed-matter systems* (Oxford University Press, 2006).
- [5] G. E. Volovik, *The universe in a helium droplet*, Vol. 117 (Oxford University Publishing, 2003).
- [6] D. Jérôme, T. Rice, and W. Kohn, *Physical Review* **158**, 462 (1967).
- [7] M. Fogler, L. Butov, and K. Novoselov, *Nature Communications* **5**, 4555 (2014).
- [8] R. Wang, O. Erten, B. Wang, and D. Xing, *Nature Communications* **10**, 210 (2019).
- [9] Z. Sun, T. Kaneko, D. Golež, and A. J. Millis, *Physical Review Letters* **127**, 127702 (2021).
- [10] X. Hu, T. Hyart, D. I. Pikulin, and E. Rossi, *Physical Review B* **105**, L140506 (2022).
- [11] Y. Shao and X. Dai, *Physical Review X* **14**, 021047 (2024).
- [12] A. A. Allocca and N. R. Cooper, *Physical Review Research* **6**, 033199 (2024).
- [13] H.-Y. Xie, P. Ghaemi, M. Mitrano, and B. Uchoa, *Proceedings of the National Academy of Sciences* **121**, e2401644121 (2024).
- [14] A. A. High, J. R. Leonard, A. T. Hammack, M. M. Fogler, L. V. Butov, A. V. Kavokin, K. L. Campman, and A. C. Gossard, *Nature* **483**, 584 (2012).
- [15] L. Du, X. Li, W. Lou, G. Sullivan, K. Chang, J. Kono, and R.-R. Du, *Nature Communications* **8**, 1971 (2017).
- [16] J. Li, T. Taniguchi, K. Watanabe, J. Hone, and C. Dean, *Nature Physics* **13**, 751 (2017).
- [17] Z. Wang, D. A. Rhodes, K. Watanabe, T. Taniguchi, J. C. Hone, J. Shan, and K. F. Mak, *Nature* **574**, 76 (2019).
- [18] L. Ma, P. X. Nguyen, Z. Wang, Y. Zeng, K. Watanabe, T. Taniguchi, A. H. MacDonald, K. F. Mak, and J. Shan, *Nature* **598**, 585 (2021).
- [19] J. Gu, L. Ma, S. Liu, K. Watanabe, T. Taniguchi, J. C. Hone, J. Shan, and K. F. Mak, *Nature physics* **18**, 395 (2022).
- [20] Y. Jia, P. Wang, C.-L. Chiu, Z. Song, G. Yu, B. Jäck, S. Lei, S. Klemenz, F. A. Cevallos, M. Onyszczak, *et al.*, *Nature Physics* **18**, 87 (2022).
- [21] J. Huang, B. Jiang, J. Yao, D. Yan, X. Lei, J. Gao, Z. Guo, F. Jin, Y. Li, Z. Yuan, *et al.*, *Physical Review X* **14**, 011046 (2024).
- [22] P. Zhang, Y. Dong, D. Yan, B. Jiang, T. Yang, J. Li, Z. Guo, Y. Huang, Q. Li, Y. Li, *et al.*, *Physical Review X* **14**, 011047 (2024).
- [23] B. A. Bernevig, T. L. Hughes, and S.-C. Zhang, *Science* **314**, 1757 (2006).
- [24] H. Zhang, C.-X. Liu, X.-L. Qi, X. Dai, Z. Fang, and S.-C. Zhang, *Nature Physics* **5**, 438 (2009).
- [25] Z. Zhu, Y. Cheng, and U. Schwingenschlögl, *Physical Review B* **85**, 235401 (2012).
- [26] D. Thouless, *Journal of Physics C: Solid State Physics* **17**, L325 (1984).
- [27] C. Brouder, G. Panati, M. Calandra, C. Mourougane, and N. Marzari, *Physical Review Letters* **98**, 046402 (2007).
- [28] H. Yang, J. Zeng, Y. Shao, Y. Xu, X. Dai, and X.-Z. Li, *Physical Review B* **109**, 075167 (2024).
- [29] MTCO is a member of the family of MXenes, 2D materials whose prospect for topological and highly correlated phenomena has generated increasing interest in recent years [58–65].
- [30] Z. Jiang, Y. Li, S. Zhang, and W. Duan, *Physical Review B* **98**, 081408 (2018).
- [31] S. S. Ataie, D. Varsano, E. Molinari, and M. Rontani, *Proceedings of the National Academy of Sciences* **118**, e2010110118 (2021).
- [32] Y.-Q. Wang, M. Papaj, and J. E. Moore, *Physical Review B* **108**, 205420 (2023).
- [33] E. Davari, S. S. Ataie, and M. Kargarian, *Physical Review B* **109**, 075146 (2024).
- [34] B. Zenker, H. Fehske, and H. Beck, *Physical Review B* **90**, 195118 (2014).
- [35] In atomic units, the unit of length is given by the Bohr radius, $a_0 = 0.529\,177\,\text{Å}$, and the unit of energy is the Hartree energy, $E_h = 27.211\,386\,\text{eV}$. In particular, the momenta are expressed in units of a_0^{-1} .
- [36] S. Hirata and M. Head-Gordon, *Chemical Physics Letters* **314**, 291 (1999).
- [37] G. Onida, L. Reining, and A. Rubio, *Reviews of Modern Physics* **74**, 601 (2002).
- [38] M. Gruning, A. Marini, and X. Gonze, *Nano Letters* **9**, 2820 (2009).
- [39] T. Sander, E. Maggio, and G. Kresse, *Physical Review B* **92**, 045209 (2015).
- [40] E. Maggio and G. Kresse, *Physical Review B* **93**, 235113 (2016).
- [41] T. Sander and G. Kresse, *The Journal of Chemical Physics* **146** (2017).
- [42] F. Wu, F. Qu, and A. H. MacDonald, *Physical Review B* **91**, 075310 (2015).
- [43] L. Maisel Licerán, F. García Flórez, L. D. Siebbeles, and H. T. Stoof, *Scientific Reports* **13**, 6337 (2023).
- [44] D. Y. Qiu, T. Cao, and S. G. Louie, *Physical Review Letters* **115**, 176801 (2015).
- [45] We have solved the BSE (with and without the TDA) in polar coordinates by discretizing the momentum magnitude for different numbers of points N . The error intervals in the reported values of ΔE correspond to the uncertainties of the intercepts when extrapolating the obtained energies to the continuum by considering E as a function of $1/N$. We have used enough values of N to accurately determine the sign of ΔE .
- [46] T. Senthil, J. Marston, and M. P. Fisher, *Physical Review B* **60**, 4245 (1999).
- [47] N. Read and D. Green, *Physical Review B* **61**, 10267 (2000).
- [48] R. Jackiw and C. Rebbi, *Physical Review D* **13**, 3398 (1976).
- [49] S. Peotta and P. Törmä, *Nature Communications* **6**, 8944 (2015).
- [50] L. Liang, T. I. Vanhala, S. Peotta, T. Siro, A. Harju, and P. Törmä, *Physical Review B* **95**, 024515 (2017).
- [51] T. Kitamura, A. Daido, and Y. Yanase, *Physical Review B* **106**, 184507 (2022).
- [52] T. Kitamura, T. Yamashita, J. Ishizuka, A. Daido, and Y. Yanase, *Physical Review Research* **4**, 023232 (2022).
- [53] D. R. Nelson and J. Kosterlitz, *Physical Review Letters* **39**, 1201 (1977).
- [54] K. Furutani, G. Midei, A. Perali, and L. Salasnich, arXiv preprint arXiv:2404.15728 (2024).
- [55] M. Tam and S. Peotta, *Physical Review Research* **6**, 013256 (2024).
- [56] Y. Nagaoka and J. Yamauchi, *Solid State Communications* **17**, 693 (1975).
- [57] R. Wang, T. A. Sedrakyan, B. Wang, L. Du, and R.-R. Du,

- Nature **619**, 57 (2023).
- [58] Y. Gogotsi and B. Anasori, *ACS Nano* **13**, 8491 (2019).
- [59] M. Khazaei, A. Mishra, N. S. Venkataramanan, A. K. Singh, and S. Yunoki, *Current Opinion in Solid State and Materials Science* **23**, 164 (2019).
- [60] O. Salim, K. Mahmoud, K. Pant, and R. Joshi, *Materials Today Chemistry* **14**, 100191 (2019).
- [61] M. Naguib, M. W. Barsoum, and Y. Gogotsi, *Advanced Materials* **33**, 2103393 (2021).
- [62] A. VahidMohammadi, J. Rosen, and Y. Gogotsi, *Science* **372**, eabf1581 (2021).
- [63] S. Dong and Y. Li, *Physical Review B* **107**, 235147 (2023).
- [64] N. Kumar and F. Karlický, *Applied Physics Letters* **122** (2023).
- [65] N. Kumar, M. Kolos, S. Bhattacharya, and F. Karlický, *The Journal of Chemical Physics* **160** (2024).